 doi:10.20944/preprints201912.0247.v1

Article

Computational Improvement of Small-Molecule Inhibitors of *Bacillus anthracis* Protective Antigen Activation through Isostere-Based Substitutions.

Sandra V. R. L. Silva[1] and Pedro J. Silva [1,*]

[1] FP-ENAS/Faculdade de Ciências da Saúde, Universidade Fernando Pessoa, Rua Carlos da Maia, 296, 4200-150 Porto, Portugal

* Correspondence: pedros@ufp.edu.pt (P.J.S.)

Abstract: There has recently been interest in the development of small-molecule inhibitors of the oligomerization of *Bacillus anthracis* protective antigen for therapeutic use. Some of the proposed lead compounds have, however, unfavorable solubility in aqueous medium, which prevents their clinical use. In this computational work, we have designed several hundreds of derivatives with progressively higher hydrosolubility and tested their ability to dock the relevant binding cavity. The highest-ranking docking hits were then subjected to 125 ns-long simulations to ascertain the stability of the binding modes. Several of the potential candidates performed quite disappointingly , but two molecules showed very stable binding modes throughout the complete simulations. Besides the identification of these two promising leads, these molecular dynamics simulations allowed the discovery of several insights that shall prove useful in the further improvement of these candidate towards higher potency and stability.

Keywords: anthrax; lead compounds; molecular dynamics; docking

1. Introduction

The toxicity of *Bacillus anthracis* towards animal cells depends on the action of three proteins: a Zn^{2+} protease, an adenylcyclase and a transporting protein called "protective antigen" due to its ability to elicit protective immunity against anthrax [1]. Upon infection of a host, the N-terminal domain of the protective antigen (Figure 1, panel A) is cleaved by a host-derived protease[2–4] and the remaining product assembles into heptamers which bind the adenycyclase or Zn^{2+} protease toxin components and are endocyted[5]. In the endosome, acidification leads the heptamers into converting into membrane-spanning pores, through which the toxin components translocate into the cytosol, eventually leading to the symptoms of anthrax[6]. Treatment involves prolonged doses of antibiotics and the use of antitoxins which interact with the protective antigen and render it inoperative[7]. Another possible treatment strategy consists in the inhibition of the oligomerization of the protective antigen through the intervention of small molecules that bind protein surfaces involved in the formation of the prepore[8,9]. An *in silico* screen of a compound library identified[9] several molecules with the ability to bind a small cavity (Figure 1, panel B) in the protective antigen located at the oligomerization interface, close to the region where the N-terminal domain contacts the rest of the protein. Two of these molecules (Chembridge library members 5181401 and 5180717) were then experimentally shown to possess the ability to prevent the oligomerization and to protect cells from anthrax lethal toxin *in vitro*. Serum albumin, however, prevented these molecules from protecting the cells, suggesting that their high hydrophobicity will render them unsuitable for clinic applications. In this work, we have designed and analyzed computationally a large variety of less hydrophobic derivatives of these ligands to identify higher affinity analogues with improved clinical applicability.

Preprints (www.preprints.org) | NOT PEER-REVIEWED | Posted: 19 December 2019 doi:10.20944/preprints201912.0247.v1

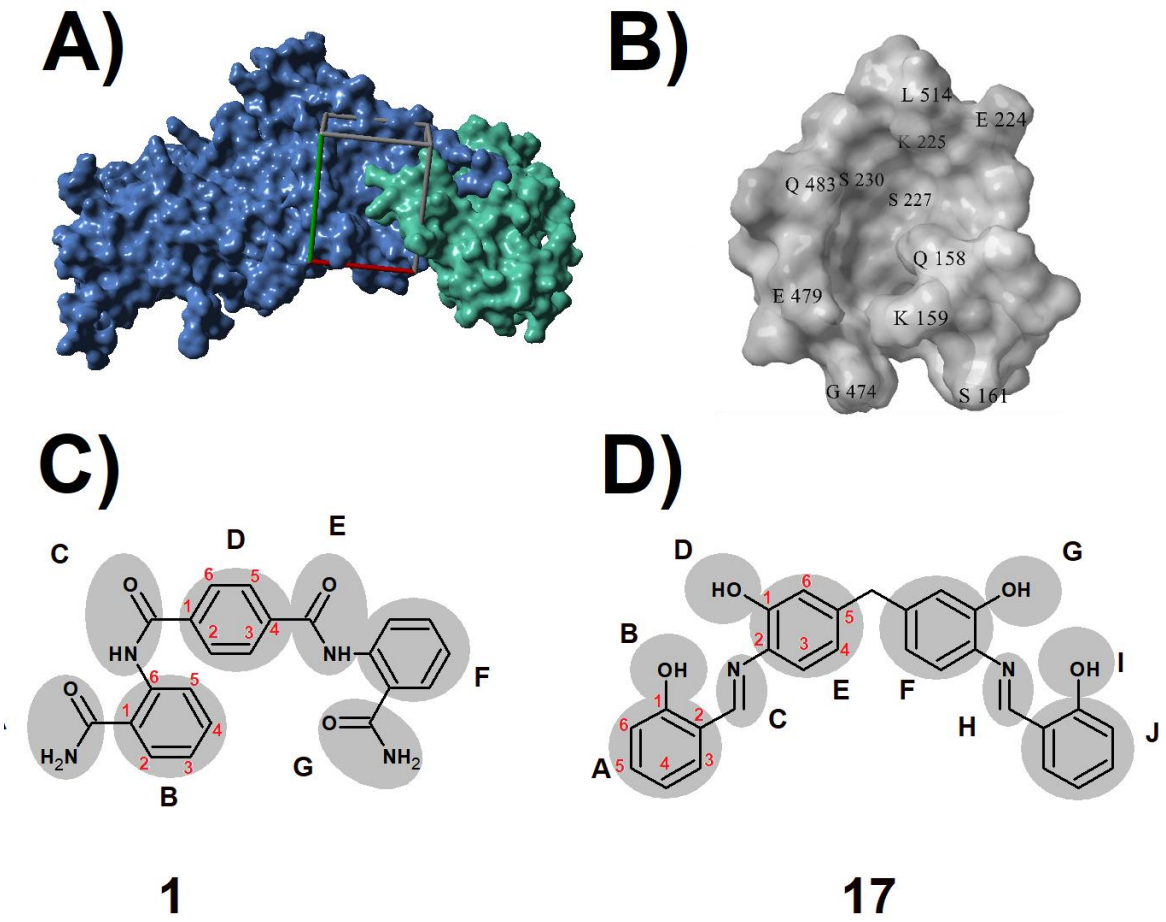

Figure 1. A) Molecular surface of the protective antigen. The N-terminal portion cleaved prior to activation is colored green. The docking site studied is highlighted with a rectangular box. B) Molecular surface of the binding site. C and D) Scaffolds used for the generation of novel inhibitor candidates: Chembridge library member 5181401 (C) and Chembridge library member 51810717 D). Regions subjected to bioisosteric modification[10,11] are highlighted. The numbering scheme used throughout the manuscript is shown in each ring. In molecule 1, the numbering of moiety F is analogous to that of moiety B. In molecule **17** , the numbering of moieties F and J are analogous to E and A, respectively.

2. Materials and Methods

All computations were performed in YASARA[12] using the 1.45 Å resolution crystal structure of the protective antigen in which the membrane-insertion loop (residues 303–324) was replaced with the Pro-Gly dipeptide, at pH=8.5 (PDB: 3TEW) (Figure 1) [13]. New inhibitor candidates (Figure 1 and Supporting Information) were generated through bioisosteric replacement[10,11] at strategic positions of the two ligands[9] found previously (Chembridge library members 5181401, henceforth referred as **1,** and 5180717, henceforth referred as **17**), and then docked with AutoDock Vina [14] using default docking parameters. The docking region was confined to a 51.0×36.7×34.5 Å box centered on the crevice between segments 159-162 and 473-485. The cavity itself (Figure 1B) is about 8 Å wide and 20 Å long and can be divided in two regions: an "exposed" lobe open to bulk solvent lined by aminoacids 224-230 and a "protected" lobe lined by aminoacids 461-464 and 472-483, partially protected from bulk solvent by a "lid" formed by the sidechains of N-terminal domain aminoacids Q158 and K159. The docking box we used is considerably larger than the cavity to

Preprints (www.preprints.org) | NOT PEER-REVIEWED | Posted: 19 December 2019 doi:10.20944/preprints201912.0247.v1

ensure that putative candidates that bound to only one of the lobes of the cavity and to the surrounding surface (instead of occupying the complete cavity) could be filtered out. The ligands with higher dissociation energies were selected for further study through molecular dynamics. All molecular dynamics simulations were run with the AMBER03 forcefield[15], using a multiple time step of 1.25 fs for intramolecular and 2.5 fs for intermolecular forces. Simulations were performed in cells 25 Å larger than the solute along each axis (final cell dimensions 159.0 × 111.9 × 124.83 Å), and counter-ions (195 Cl^- and 198 Na^+) were added to a final concentration of 0.9 % NaCl. In total, the simulations contained approximately 221,770 atoms. A 8 Å cutoff was taken for Lennard-Jones forces and the direct space portion of the electrostatic forces, which were calculated using the Particle Mesh Ewald method[16] with a grid spacing <1 Å, 4th order B-splines and a tolerance of 10^{-4} for the direct space sum. Simulated annealing minimizations started at 298 K, velocities were scaled down with 0.9 every ten steps for a total time of 5 ps. After annealing, simulations were run at 298 K. Temperature was adjusted using a Berendsen thermostat[17] based on the time-averaged temperature, i.e., to minimize the impact of temperature control, velocities were rescaled only about every 100 simulation steps, whenever the average of the last 100 measured temperatures converged. Substrate parameterization was performed with the AM1BCC protocol[18,19]. All simulations were run for at least 125 ns. Unless otherwise noted, average interaction distances and standard deviations were computed on the whole trajectory after discarding the initial 15 ns.

3. Results

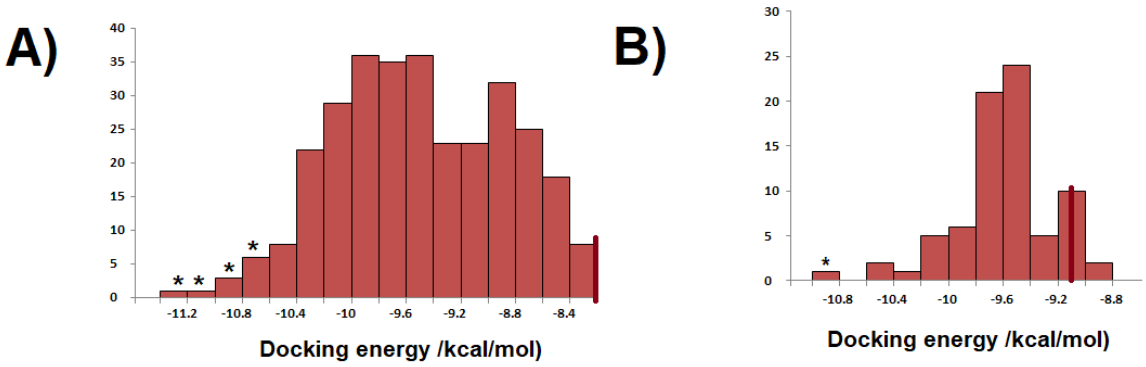

Figure 2. A) Distribution of the docking energies of the derivatives Chembridge library member 51810717. B) Distribution of the docking energies of the derivatives Chembridge library member 5181401. In both histograms, the energy of the unmodified library member is shown as a thick red line. In each histogram, an asterisk highlights the bins from which a candidate structure was analyzed through molecular dynamics simulations.

305 derivatives of Chembridge library member **17** and 76 derivatives of Chembridge library member **1** were designed and docked to the target cavity. Our modifications of **17** usually involved the increase of dipole moment of the rings through substitution of carbon by nitrogen or addition of halogen atoms, the reduction of one of the imine bonds or the replacement of phenolic hydroxyl groups by non-classical bioisosteres. The tested modifications invariably improved the docking energy (Figure 2A), showing that ample room exists for improvement of the binding capabilities of **17**. Modifications of **1** were not always as effective in improving the docking energy: replacing one of the amides by an acetyl group, appending a single methylamine group on the D ring (Figure 1) or replacing one of the phenyl carbons by nitrogen yielded compounds with slightly worse binding ability than the original compound. Only one derivative of **1** (1-67) had an improvement above 1.5 kcal/mol over the original compound, whereas the improvement over **17** was much more extensive, with seven molecules (Table 1) showing an improvement above 2.6 kcal/mol. Surprisingly, the effects of individual substitutions on the docking energies proved not to be additive, partly due to the flexibility allowed by the large size of the lobes of the binding cavity and partly due to the high

Preprints (www.preprints.org) | NOT PEER-REVIEWED | Posted: 19 December 2019 doi:10.20944/preprints201912.0247.v1

symmetry of the parent molecules, which allows the generation of two different molecules from the addition of two individual effects.

The scoring functions used to rank the solutions from docking experiments are well-known to be imperfect and to be able, at most, to significantly improve the likelihood that a high-ranking molecule will be a strong ligand. We therefore proceeded to analyze the stability of the binding modes of our candidate molecules through molecular dynamics simulations.

Table 1. Substitution pattern in the derivatives of **17** with the best docking energies.

Derivative	Docking energy (kcal/mol)	A	B	F	G	H	I
17-61	11.34	N^6		6-fluoro- 2,4-CHD			
17-283	11.04	N^6		6-hidroxy-2,4-CHD			
17-275	10.90	N^6		6-chloro-2,4 CHD			
17-288	10.84	N^6					-NH-C=O-O-
17-239	10.83	N^6		2,4 CHD			
17-147	10.78	N^6O^5-2,6 CHD		F^6			-NH-C=O-NH-
17-222	10.77	HN^6	=O	2,4-CHD	=O	$-NH_2^+-CH_2$	-NH-C=O-O-

Legend: 2,4-CHD: 2,4-cyclohexadiene; 2,6 CHD: cyclohexadiene with double bond between atoms 2 and 3 and between atoms 1 and 6; N^6: replacement of a -HC= at position 6 by -N=.

2.1. Candidate 1-67

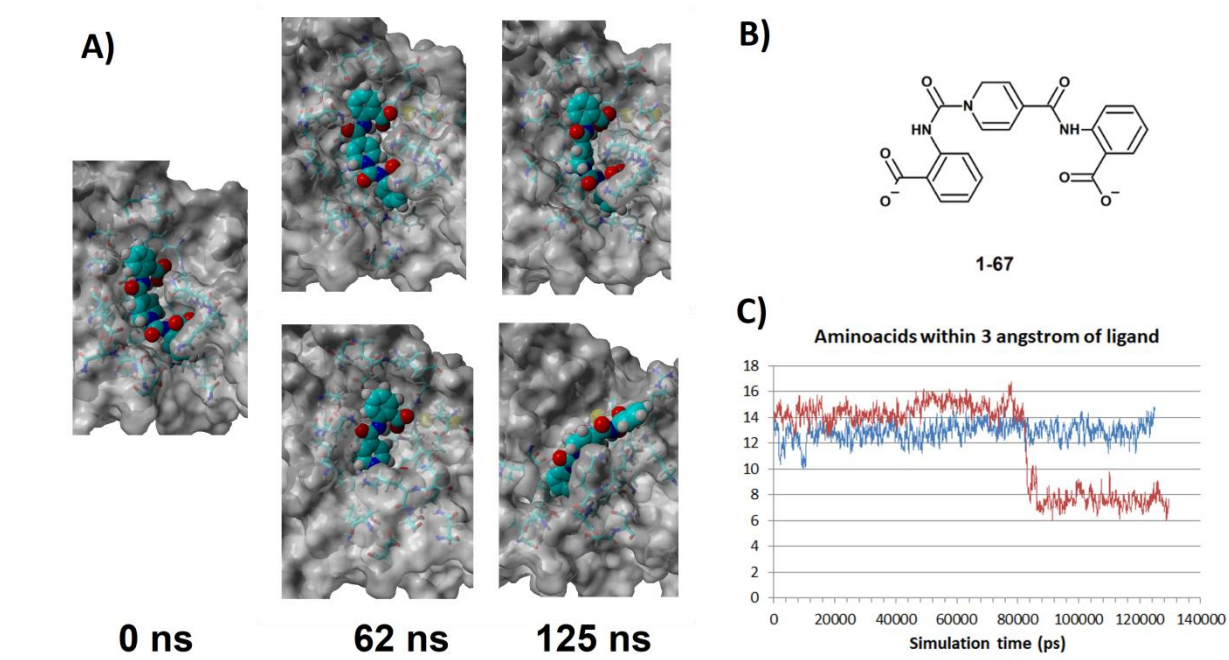

Figure 3. A) Evolution of the binding mode of 1-67 along two different simulations started from the same binding pose. Ligand unbinding is evident at 125 ns in one simulation (upper panels), whereas stable binding is seen in the other simulation (lower panels) B) Chemical structure of candidate 1-67.

Preprints (www.preprints.org) | NOT PEER-REVIEWED | Posted: 19 December 2019 doi:10.20944/preprints201912.0247.v1

C) Evolution of protein-ligand contacts along the two simulations (moving average of 200ps windows centered on the graphed points). Upper simulation: blue trace; Lower simulation: red trace

1-67 (Figure 3B) differs from the original ligand **1** in the replacement of both amide groups by carboxylates and by the presence of a nitrogen in the central ring, which increases its dipole moment. In the initial binding pose, strong hydrogen bonds are established between one of its carboxylate groups and the backbone amides of Lys159 (3.63±0.50 Å)and Gln158 (2.73±0.32 Å) while the other end of the molecule is nested in the "exposed" cavity lobe lined by residues 226-232 and the carboxylate in that end interacts with the backbone amides of Ser227 (2.80±0.19 Å)and Trp226(2.39±0.50 Å) (Figure 3A). Since two very similar binding poses were obtained in the docking procedure, we analysed the stability of the complex with four 125 ns simulations (two from each binding pose). We found a similar behavior in each pair of simulations: in one instance, the complex remained stable throughout the 125 ns, whereas in the other instance the ligand started to unbind after around 80 ns (Figure 3A and 3C and Supporting Information). In both pairs of simulations, the separation of the ligand consistently proceeded through the motion of the exposed carboxylate group present in the 223-232 lobe of the cavity away from the tethering Ser226-Trp227 amides towards the bulk solvent. This separation is made possible by the open nature of this cavity, which enables large numbers of water molecules to compete with the backbone amides for the interaction with te carboxylate. In contrast, the interaction of the other carboxylate with the Lys159 (2.77±0.40 Å) and Gln 158 (2.73±0.32 Å) backbone amides is much more stable because the sidechains of Lys159 and Gln158 largely shield it from bulk solvent. The observation of a stable interaction of the whole molecule with the protein target in only half of the simulations implies that this candidate can not be relied upon to provide a dependable inhibition. Future attempts at improvement of **1-67** should therefore refrain from placing such strong hydrophilic groups in the end of the molecule interacting with this lobe of the cavity.

2.2. Candidate 17-61

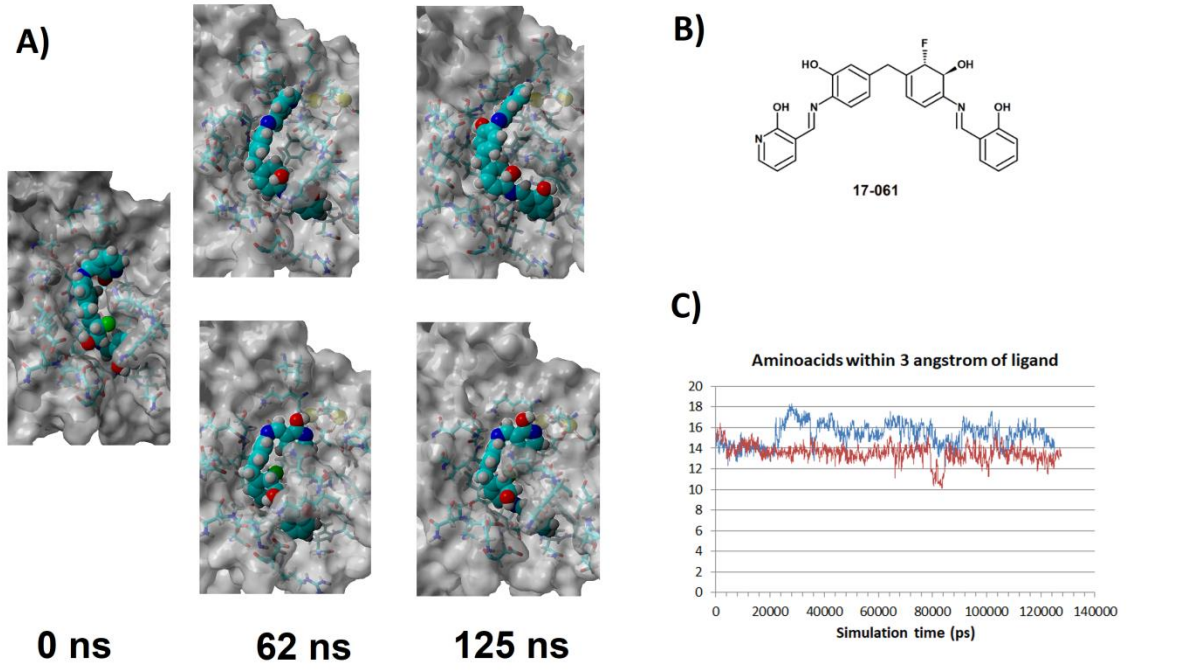

Figure 4. A) Evolution of the binding mode of 17-61 along two different simulations started from the same binding pose. B) Chemical structure of candidate 17-61. C) Evolution of protein-ligand contacts along the two simulations (moving average of 200ps windows centered on the graphed points). Upper simulation: blue trace; Lower simulation: red trace

Preprints (www.preprints.org) | NOT PEER-REVIEWED | Posted: 19 December 2019 doi:10.20944/preprints201912.0247.v1

The first analogue of 17 we studied more thoroughly (candidate 17-061) differs from the original molecule by the elimination of aromaticity in moiety F, the introduction of a halogen in that ring to increase dipole moment and in the replacement of the benzene ring in moiety A by a pyridine. In the docking pose identified by VINA, the pyridine ring lies in the "open" lobe of the cavity and the hydroxyl in moiety D forms a hydrogen bond with the carbonyl of Ser230. The ring bearing the halogen is sandwiched between Gln158 and Lys159 and the terminal phenol ring lies in the "protected" lobe of the binding site (Figure 4). Two independent simulations started from this configuration showed that the binding is very stable, although the details may change considerably. In both instances the initial hydroxyl–Ser230 carbonyl interaction is maintained throughout the simulation (2.70±0.62 Å in the first simulation, 3.17±0.59 Å in the second simulation) but other interactions are different between simulations (Figure 5): in the first case, the pyridine nitrogen remains bound to the Trp226 backbone amide (2.37±0.27 Å) while the backbone amide of Ser227 locks the hydroxy in moiety B in place (2.14±0.21 Å), while in the second simulation these interactions are absent but a transient hydrogen bond between Ser475 and the hydroxyl in moiety D is present in more than 60% of the time (2.90±1.70 Å in the full simulation, 1.98±0.19 Å if the intervals with distance >3 Å are ommited).

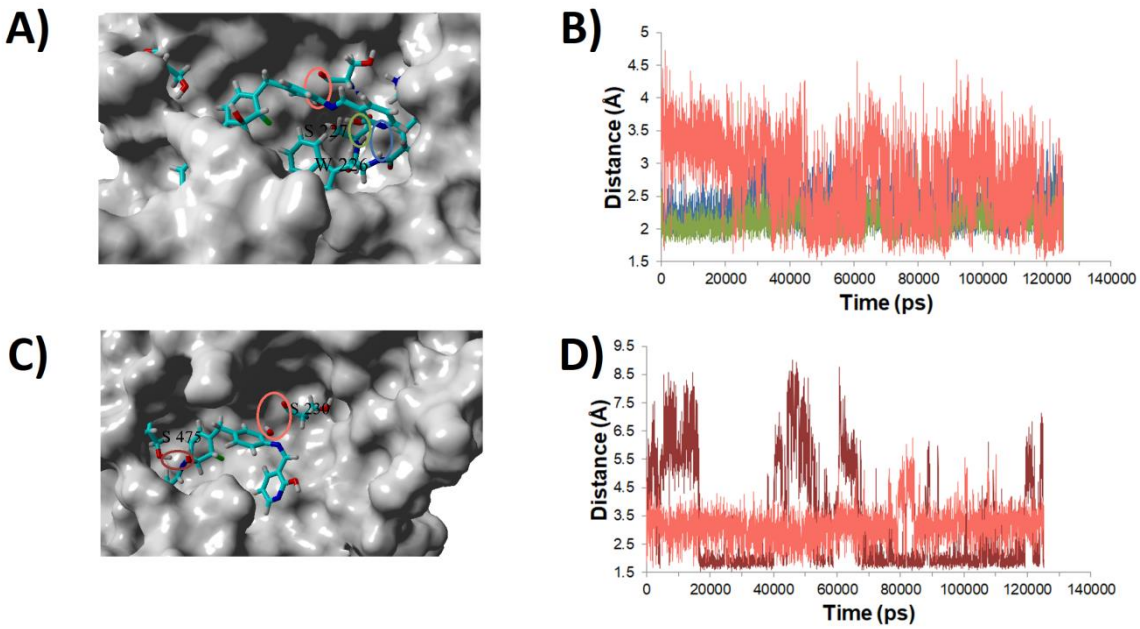

Figure 5. A) Representative snapshot of the binding mode found in the first simulation of the complex with 17-61. The binding cavity is shown from above, after Gln158 and Gln 483 have been removed for clarity. Binding interactions are highlighted with colored ellipses. B) Evolution of the stable hydrogen bonds in the first simulation. Color code is the same as the one used in panel A. C) Representative snapshot of the binding mode found in the second simulation of the complex with 17-61. The binding cavity is shown from above, after Gln158, Trp226, Ser227 and Gln 483 have been removed for clarity. Binding interactions are highlighted with colored ellipses. D) Evolution of the stable hydrogen bonds in the second simulation. Color code is the same as the one used in panel C

2.3. Candidate 17-222

Preprints (www.preprints.org) | NOT PEER-REVIEWED | Posted: 19 December 2019 doi:10.20944/preprints201912.0247.v1

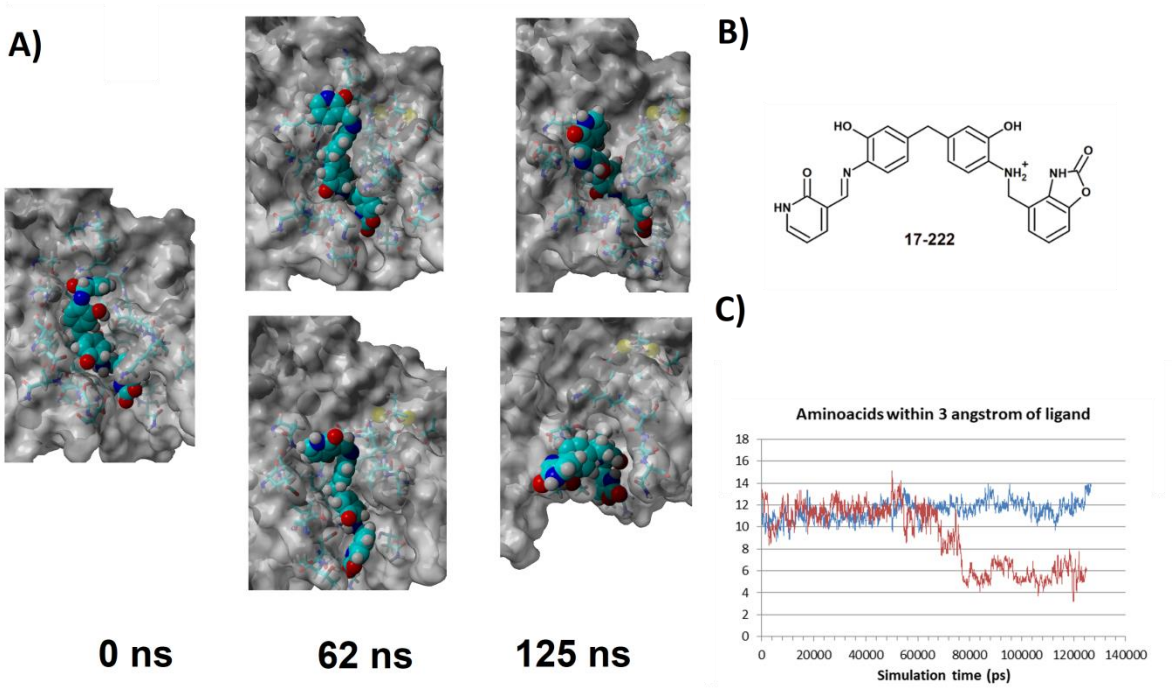

Figure 6. A) Evolution of the binding mode of 17-222 along two different simulations started from the same binding pose. B) Chemical structure of candidate 17-222. C) Evolution of protein-ligand contacts along the two simulations (moving average of 200ps windows centered on the graphed points). Upper simulation: blue trace; Lower simulation: red trace

Candidate 17-222 differs from 17-061 in the tautomeric form of the iminol in one of the extremities and in the existence of a much more hydrophilic character in the opposite end, which bears a basic amine instead of an amine and an internal carbamate group instead of the phenol hydroxide. In the initial binding pose, this hydrophilic end binds to the protected lobe, while the other end binds to the solvent-exposed portion of the cavity (Figure 6). In the first simulation an extremely stable binding mode was observed, maintained (in the protected lobe) through hydrogen bonds between the polar hydrogen attached to the internal carbamate nitrogen and Thr461 (1.97± 0.15 Å) , the protonated amine and Ser475 (2.02± 0.41 Å), and between the protonated amine and the carbonyl group of Pro232 (2.38± 0.39 Å). As observed with other candidate molecules, considerable mobility is observed in the end of the candidate interacting with the open lobe. In the second simulation a similar behaviorwas observed, though only up until 49 ns: at this moment a rotation of the protonated amine C-N bond breaks the hydrogen bond between it and the Pro232 carbonyl, and the increased flexibility leads (1.3 ns later) to the severing of the interaction of the internal carbamate moiety with Thr461. This hydrophilic site immediately interacts with the surrounding bulk water and promptly wriggles away from the cavity through the lateral opening between Gly474 and Ser161 (Figure 6).

2.4. Candidate 17-239

Preprints (www.preprints.org) | NOT PEER-REVIEWED | Posted: 19 December 2019 doi:10.20944/preprints201912.0247.v1

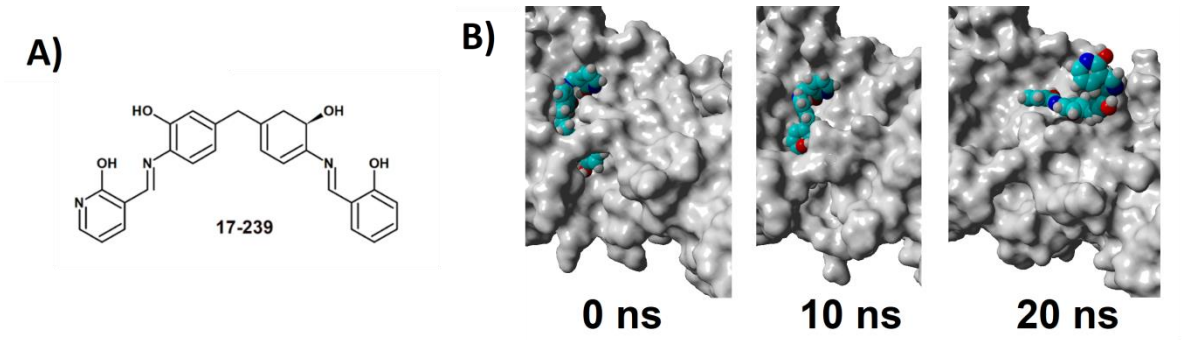

Figure 7. A) Chemical structure of candidate 17-239. B) Evolution of the binding mode of 17-239.

The structure of candidate 17-239 is very similar to that of the promising 17-61 molecule discussed earlier: the only difference lies in the absence of a halogen in the ring we called "moiety F" (Table 1 and Figure 7A). Its behavor in the binding cavity is, however, dramatically different: two hydrogen bonds between the phenol hydrogen in moiety J and the hydroxyl in moiety G with the sidechain of Ser475 are the only stable interactions between the ligand and the cavity surface. There interactions weaken dramatically after only 12 ns, and the molecule promptly leaves, though always interacting weakly with the protein surface instead of being released to the bulk.

2.5. Candidate 17-275

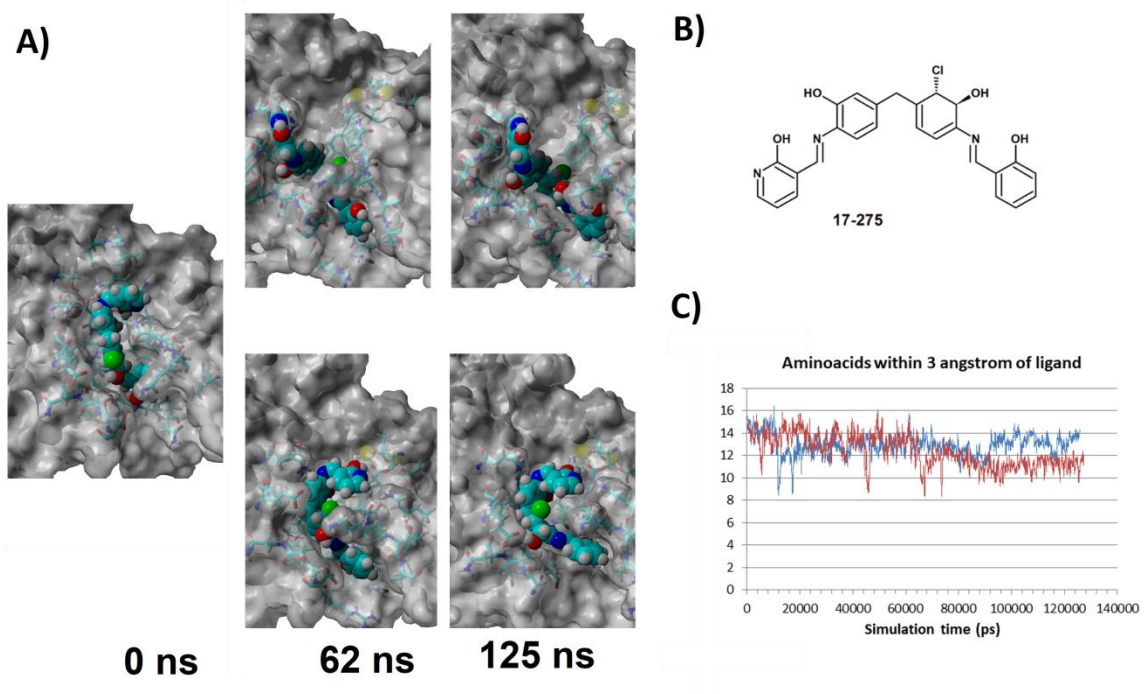

Figure 8. A) Evolution of the binding mode of 17-275 along two different simulations started from the same binding pose. B) Chemical structure of candidate 17-275. C) Evolution of protein-ligand contacts along the two simulations (moving average of 200ps windows centered on the graphed points). Upper simulation: blue trace; Lower simulation: red trace.

Molecule 17-275 differs from 17-61 and 17-239 in the presence of a chlorine atom in the position adjacent to the moiety G hydroxyl (Figure 8B). The initial docking pose, like that of those candidates, has ring F lying between the sidechains of Gln158 and Lys159 and the pyridine ring in the "open" lobe close to the Ser230 carbonyl. Both simulations yield stable, though different, binding modes. In

Preprints (www.preprints.org) | NOT PEER-REVIEWED | Posted: 19 December 2019 doi:10.20944/preprints201912.0247.v1

the first simulation (Figure 9A) the hydroxyl in moiety G interacts with the sidechain of Ser475 (O···O distance of 2.96± 0.73 Å) while the hydroxyl in moiety D establishes a hydrogen bond with the backbone amide of Asn476 (O···N distance of 3.36± 0.53 Å). Marginally less frequent interactions are present between the hydroxyl in moiety B and the Ser160 carbonyl (3.18± 0.76 Å) and between the chlorine and the Gln158 backbone amide (3.11± 0.35 Å). The second simulation visits two distinct binding modes: until 60 ns (Figure 9B), the ligand is hydrogen-bonded to the sidechain ot Thr461 (O···O distance of 3.39± 0.80 Å). After that moment, the molecule is kept in place mostly through steric interactions until a new hydrogen bond between Ser475 and the hydroxyl in moiety G (Figure 9C) forms at 86 ns (O···O distance of 2.83± 0.39 Å).

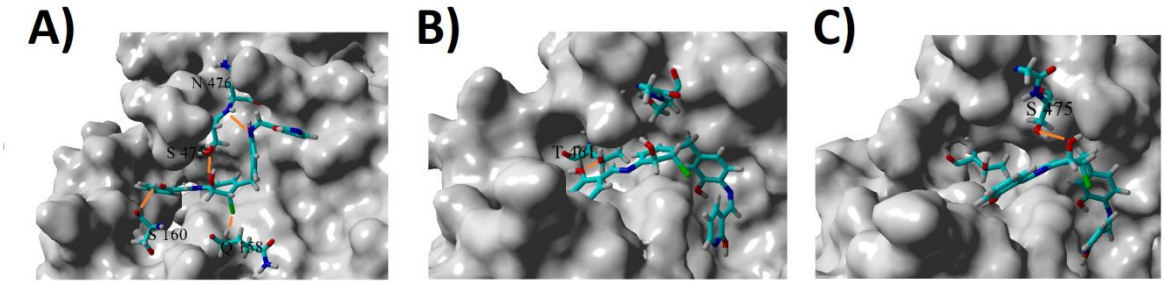

Figure 9. The three binding modes visited by candidate 17-275. Lys159 has been deleted for clarity. A) Stable pose obtained in the first simulation. Stabilizing hydrogen bonds shown in orange. B) Binding mode obtained in the first 60 ns of the second simulation. C) Binding mode obtained after 86 ns of the second simulation.

4. Discussion

Our molecular dynamics simulations clearly show that several of the good candidates identified in the docking stage are not promising leads for further development. Problematic features include the presence of concentrated charges in the moiety which binds to the "open" lobe of the cavity (as seen with candidate 01-67) as well as excessive hydrogen-bonding potential in the moiety that binds the solvent-exposed opening between Ser161 and Gly 474 in the "protected" lobe of the cavity (as observed in candidate 17-222). These observations showed us that the high-ranking molecules 17-288 and 17-147 (Table 1) are most unlikely to be good candidates and therefore we did not expend any effort with expensive molecular dynamics simulations of their binding modes. In contrast, the transformation of the aromatic ring in moiety F into a cyclohexadiene bearing two electronegative substituents afforded molecules with very good binding behavior. The good results obtained with the fluoro- and the chloro-subsituted molecules (17-61 and 17-275, respectively) strongly suggest that the hydroxy-substituted molecule 17-283, which we did not simulate due to its extreme stereoelectronic and geometric similarity to these molecules, should also be a very good candidate for further development. The lack of the second electronegative substituent in the cyclohexadiene ring (as in 17-239) has dramatic effects on the binding ability. Such a strong effect shows that the dipole interactions of this moiety with Gln158 and Lys159 (which are present in 17-61 and 17-275 but greatly decreased in 17-239) function as a critical anchor imparting stability to the complexes.

5. Conclusions

Judicious bioisosteric substitutions led to the generation of several promising improved derivatives of two previously identified inhibitors, Chembridge library members 5181401 and 5180717. Molecular dynamics simulations of the obtained docking poses showed that several of the putative complexes were less stable than desired due to the excessive hydrophilicity introduced in

the molecule by our substitutions. Two of the generated derivatives of Chembridge library member 5180717, which featured the replacement of a phenyl ring by a halogen-substituted cyclohexadiene, did result in very strong, stable, binding in repeated simulations, and show therefore good promise fro therapeutic use. Simulations of both the successful and the unsuccessful candidates additionally helped to identify several features of the active site important for the obtention of successful binding. This work further highlights the critical importance of molecular dynamics in the confirmation of the plausibility of a binding candidate identified through docking[20].

Supplementary Materials: The following are available online, Full coordinates of the docking poses of every tested candidate.

Author Contributions: conceptualization, P.S.; methodology, P.S. and V.S; formal analysis, P.S. and V.S; writing—original draft preparation, P.S.

Funding: This work was performed using computational resources acquired under project PTDC/QUI-QUI/111288/2009 and funded by FEDER through Programa Operacional Factores de Competitividade – COMPETE and by Portuguese Funds through FCT – Fundação para a Ciência e a Tecnologia.

Conflicts of Interest: The authors declare no conflict of interest. The funders had no role in the design of the study; in the collection, analyses, or interpretation of data; in the writing of the manuscript, or in the decision to publish the results.

References

1. Young, J.A.T.; Collier, R.J. Anthrax toxin: receptor binding, internalization, pore formation, and translocation. *Annu. Rev. Biochem.* **2007**, *76*, 243–65.
2. Gordon, V.; Klimpel, K. Proteolytic activation of bacterial toxins by eukaryotic cells is performed by furin and by additional cellular proteases. *Infect. Immun.* **1995**, *63*, 82–87.
3. Klimpel, K.; Molloy, S. Anthrax toxin protective antigen is activated by a cell surface protease with the sequence specificity and catalytic properties of furin. *Proc. …* **1992**, *89*, 10277–10281.
4. Gordon, V.; Rehemtulla, A.; Leppla, S. A role for PACE4 in the proteolytic activation of anthrax toxin protective antigen. *Infect. Immun.* **1997**, *65*.
5. Abrami, L.; Liu, S.; Cosson, P.; Leppla, S.H.; Van der Goot, F.G. Anthrax toxin triggers endocytosis of its receptor via a lipid raft-mediated clathrin-dependent process. *J. Cell Biol.* **2003**.
6. Miller, C.J.; Elliott, J.L.; Collier, R.J. Anthrax protective antigen: prepore-to-pore conversion. *Biochemistry* **1999**, *38*, 10432–41.
7. Hendricks, K.A.; Wright, M.E.; Shadomy, S. V.; Bradley, J.S.; Morrow, M.G.; Pavia, A.T.; Rubinstein, E.; Holty, J.-E.C.; Messonnier, N.E.; Smith, T.L.; et al. Centers for Disease Control and Prevention Expert Panel Meetings on Prevention and Treatment of Anthrax in Adults. *Emerg. Infect. Dis.* **2014**, *20*.
8. Rubert Pérez, C.; López-Pérez, D.; Chmielewski, J.; Lipton, M. Small Molecule Inhibitors of Anthrax Toxin-induced Cytotoxicity Targeted Against Protective Antigen. *Chem. Biol. Drug Des.* **2012**, *79*, 260–269.
9. Wein, A.N.; Williams, B.N.; Liu, S.; Ermolinsky, B.; Provenzano, D.; Abagyan, R.; Orry, A.; Leppla, S.H.; Peredelchuk, M. Small molecule inhibitors of Bacillus anthracis protective antigen proteolytic activation and oligomerization. *J. Med. Chem.* **2012**, *55*, 7998–8006.
10. Patani, G.A.; LaVoie, E.J. Bioisosterism: A Rational Approach in Drug Design. *Chem. Rev.* **1996**, *96*, 3147–3176.

 doi:10.20944/preprints201912.0247.v1

11. Meanwell, N. a Synopsis of some recent tactical application of bioisosteres in drug design. *J. Med. Chem.* **2011**, *54*, 2529–91.
12. Krieger, E.; Darden, T.; Nabuurs, S.B.; Finkelstein, A.; Vriend, G. Making optimal use of empirical energy functions: Force-field parameterization in crystal space. *Proteins-Structure Funct. Bioinforma.* **2004**, *57*, 678–683.
13. Feld, G.K.; Kintzer, A.F.; Tang, I.I.; Thoren, K.L.; Krantz, B. a Domain flexibility modulates the heterogeneous assembly mechanism of anthrax toxin protective antigen. *J. Mol. Biol.* **2012**, *415*, 159–74.
14. Trott, O.; Olson, A.J. AutoDock Vina: improving the speed and accuracy of docking with a new scoring function, efficient optimization, and multithreading. *J. Comput. Chem.* **2010**, *31*, 455–61.
15. Duan, Y.; Wu, C.; Chowdhury, S.; Lee, M.C.; Xiong, G.; Zhang, W.; Yang, R.; Cieplak, P.; Luo, R.; Lee, T.; et al. A point-charge force field for molecular mechanics simulations of proteins based on condensed-phase quantum mechanical calculations. *J. Comput. Chem.* **2003**, *24*, 1999–2012.
16. Essmann, U.; Perera, L.; Berkowitz, M.L.; Darden, T.; Lee, H.; Pedersen, L.G. A smooth particle mesh Ewald method. *J. Chem. Phys.* **1995**, *103*, 8577–8593.
17. Berendsen, H.J.C.; Postma, J.P.M.; van Gunsteren, W.F.; DiNola, A.; Haak, J.R. Molecular dynamics with coupling to an external bath. *J. Chem. Phys.* **1984**, *81*, 3684.
18. Jakalian, A.; Bush, B.L.; Jack, D.B.; Bayly, C.I.; I, A.C.A.M. Fast, efficient generation of high-quality atomic charges. AM1-BCC model: I. Method. *J. Comput. Chem.* **2000**, *21*, 132–146.
19. Jakalian, A.; Jack, D.B.; Bayly, C.I. Fast, efficient generation of high-quality atomic charges. AM1-BCC model: II. Parameterization and validation. *J. Comput. Chem.* **2002**, *23*, 1623–1641.
20. Chen, Y. Beware of docking! *Trends Pharmacol. Sci.* **2015**, *36*, 78–95.